electronics

MDPI

Article

Applying Data Mining and Artificial Intelligence Techniques for High Precision Measuring of the Two-Phase Flow's Characteristics Independent of the Pipe's Scale Layer

Abdulilah Mohammad Mayet [1], Ahmed S. Salama [2], Seyed Mehdi Alizadeh [3], Slavko Nesic [4], John William Grimaldo Guerrero [5,*], Ehsan Eftekhari-Zadeh [6,*], Ehsan Nazemi [7] and Abdullah M. Iliyasu [8,9,10,*]

1 Electrical Engineering Department, King Khalid University, Abha 61411, Saudi Arabia; amayet@kku.edu.sa
2 Faculty of Engineering and Technology, Future University in Egypt, Cairo 11835, Egypt; asalama@fue.edu.eg
3 Petroleum Engineering Department, Australian College of Kuwait, West Mishref 13015, Kuwait; s.alizadeh@ack.edu.kw
4 Faculty of Technology, University of Novi Sad, 21000 Novi Sad, Serbia; slavko.nesic@nis.rs
5 Department of Energy, Universidad de la Costa, Barranquilla 080001, Colombia
6 Institute of Optics and Quantum Electronics, Friedrich-Schiller-University Jena, Max-Wien-Platz 1, 07743 Jena, Germany
7 Imec-Vision Laboratory, University of Antwerp, 2610 Antwerp, Belgium; ehsan.nazemi@uantwerpen.be
8 College of Engineering, Prince Sattam Bin Abdulaziz University, Al-Kharj 11942, Saudi Arabia
9 School of Computing, Tokyo Institute of Technology, Yokohama 226-8502, Japan
10 School of Computer Science and Technology, Changchun University of Science and Technology, Changchun 130022, China
* Correspondence: jgrimald1@cuc.edu.co (J.W.G.G.); e.eftekharizadeh@uni-jena.de (E.E.-Z.); a.iliyasu@psau.edu.sa (A.M.I.)

check for updates

Citation: Mayet, A.M.; Salama, A.S.; Alizadeh, S.M.; Nesic, S.; Guerrero, J.W.G.; Eftekhari-Zadeh, E.; Nazemi, E.; Iliyasu, A.M. Applying Data Mining and Artificial Intelligence Techniques for High Precision Measuring of the Two-Phase Flow's Characteristics Independent of the Pipe's Scale Layer. *Electronics* **2022**, *11*, 459. https://doi.org/10.3390/electronics11030459

Academic Editor: Grzegorz Dudek

Received: 13 January 2022
Accepted: 2 February 2022
Published: 3 February 2022

Abstract: Scale formation inside oil and gas pipelines is always one of the main threats to the efficiency of equipment and their depreciation. In this study, an artificial intelligence method method is presented to provide the flow regime and volume percentage of a two-phase flow while considering the presence of scale inside the test pipe. In this non-invasive method, a dual-energy source of barium-133 and cesium-137 isotopes is irradiated, and the photons are absorbed by a detector as they pass through the test pipe on the other side of the pipe. The Monte Carlo N Particle Code (MCNP) simulates the structure and frequency features, such as the amplitudes of the first, second, third, and fourth dominant frequencies, which are extracted from the data recorded by the detector. These features use radial basis function neural network (RBFNN) inputs, where two neural networks are also trained to accurately determine the volume percentage and correctly classify all flow patterns, independent of scale thickness in the pipe. The advantage of the proposed system in this study compared to the conventional systems is that it has a better measuring precision as well as a simpler structure (using one detector instead of two).

Keywords: pipeline's scale; RBF neural network; two-phase flow; oil and gas; artificial intelligence

1. Introduction

The need to continue drilling or stopping, optimizing the separation process, how the extracted material is transported, and many other things depend on recognizing the flow pattern and volume fraction of each component. Gamma radiation is used for the detection, although hydrostatic, ultrasonic, and hydrometric techniques can also be used to detect the flow pattern and volume fraction of the multiphase flow. In 1999, Abro et al. conducted one of the first studies in this field to determine the volume percentage [1]. The use of the low-energy gamma-ray of americium-241 instead of the traditional source of caesium-137, and the use of three detectors at 140°, −154°, and 180° relative to the source to find the optimal position of the detector, were the most positive and creative points of the study. Sattari et al. presented a study in 2020 by decreasing the number of detectors to one and using two independent GMDH neural networks to determine the percentage of volume fraction and flow regime [2]. The simulation of three common flow patterns, namely annular, homogeneous, and stratified, in void fractions of 5% to 90% was done by removing the noise of the extracted photon spectrum using a Savitzky−Golay filter and providing the filter output as the input of the neural network. The approach in the study of Sattari et al. ultimately predicted the volume percentage and type of flow regime with a root mean square error (RMSE) less than 1.11; however, oil and gas transmission pipes sometimes deposit scale after a period of use, which was not investigated in this study. Studies have been conducted in recent years to identify these scales and to make the mentioned predictions. In 2015, Oliveira et al. conducted a pipeline survey using a structure that was included a detector and a cesium-137 energy source [3]. The process was such that the source and the detector were continuously shifted 5 mm at the same time, and the detector received radiation emitted from the source for 60 s. The results proved that the presence or absence of scales, as well as their thickness, can be predicted with good accuracy. In [4], the researchers were able to model flow patterns in different volume percentages and thickness scales using the SVM network, and to classify the flow regimes with a not so high accuracy. The volume percentage was also calculated with an RMSE of less than 3.67. Alamoudi et al. attempted to develop a gamma attenuation technique using RBFNN to determine the scale thickness of oil pipelines where two-phase flow with various symmetric patterns and volume fractions exist [5]. The applications of artificial intelligence in multiphase flowmeters have been discussed in many studies to date, some of which can be found in [6–15]. In pipelines, valves, and pumps used in the production and processing of oil, scales may form over time. The formation of scales leads to the blockage and obstruction of the flow of fluid. At this time, the oilfield scale inhibition process becomes important. These deposits lead to a reduction in the inner diameter of the pipe and consequently cause a reduction in the life of the equipment, reducing efficiency, and ultimately increasing costs [16]. In [17], the researchers implemented a structure consisting of a dual- energy gamma source to detect the type of flow regimes independent of scale thickness. Although these important parameters were predicted with an acceptable accuracy, the use of two detectors increased the cost and complexity of the detection system. An example of scale deposition in the oil pipe is shown in Figure 1.

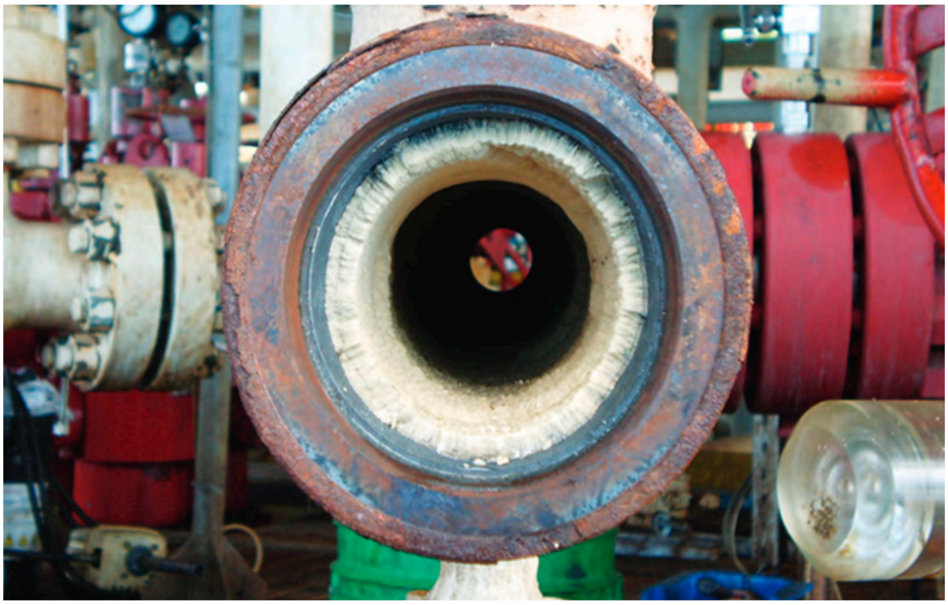

Figure 1. Example of scale deposition in a pipe.

2. Simulation Setup

The modeling of the detection system in this study was performed using version X of the Monte Carlo N-Particle Code (MCNPX) [18]. The schematic configuration of the above-mentioned detection system is demonstrated in Figure 2. As is apparent, this schematic diagram uses the stratified flow as an example. The dual-energy source is on the left, a pipe in which two-phase flows and scales are formed in it is on the middle, and an NaI detector to receive the transmitted photons is on the right.

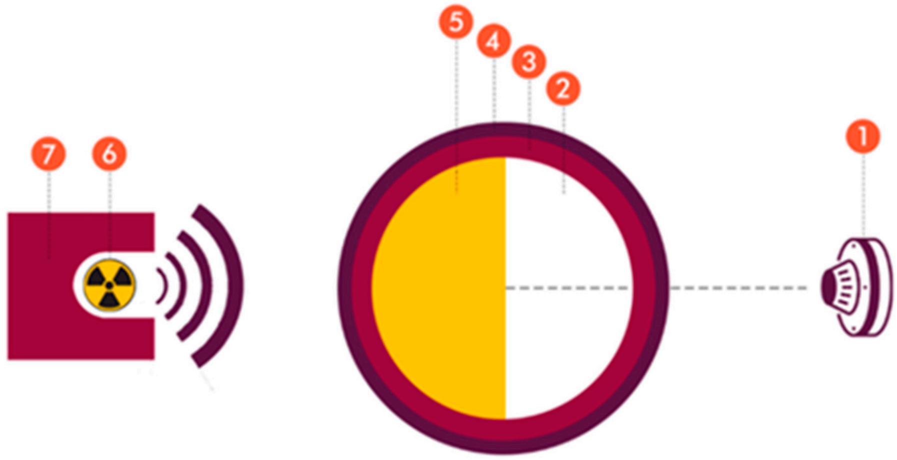

Figure 2. Simulated detection system: (1) NaI detector; (2) gas phase; (3) formed scale; (4) steel pipe; (5) liquid phase; (6) dual-energy source; (7) shield.

The disk source defined for modeling the radiation source. It was located inside a shield to move the beams toward the transmission detector. The source includes two radioisotopes of cesium-137 and barium-133, which acted at 0.662 MeV and 0.356 MeV, respectively. In the proposed structure, just in front of the photon emission source, a 25.4 mm NaI detector was placed to receive the passing photons. Three annular, stratified, and homogeneous flow regimes were simulated by 15% steps in 10% to 85% volumetric percentages with 7 different scale thicknesses (0, 0.5, 1, 1.5, 2, 2.5, and 3 cm). These three regimes are illustrated in Figure 3.

Figure 3. Simulated flow regimes from left to right: stratified, homogeneous, and annular, respectively.

In this study, a steel pipe with inner diameter of 20 cm was selected. The scale inside the pipe was a symmetrical circular layer of $BaSO_4$ with different thicknesses. The depiction of the recorded spectra for three flow patterns and different gas volume percentages is apparent in Figure 4.

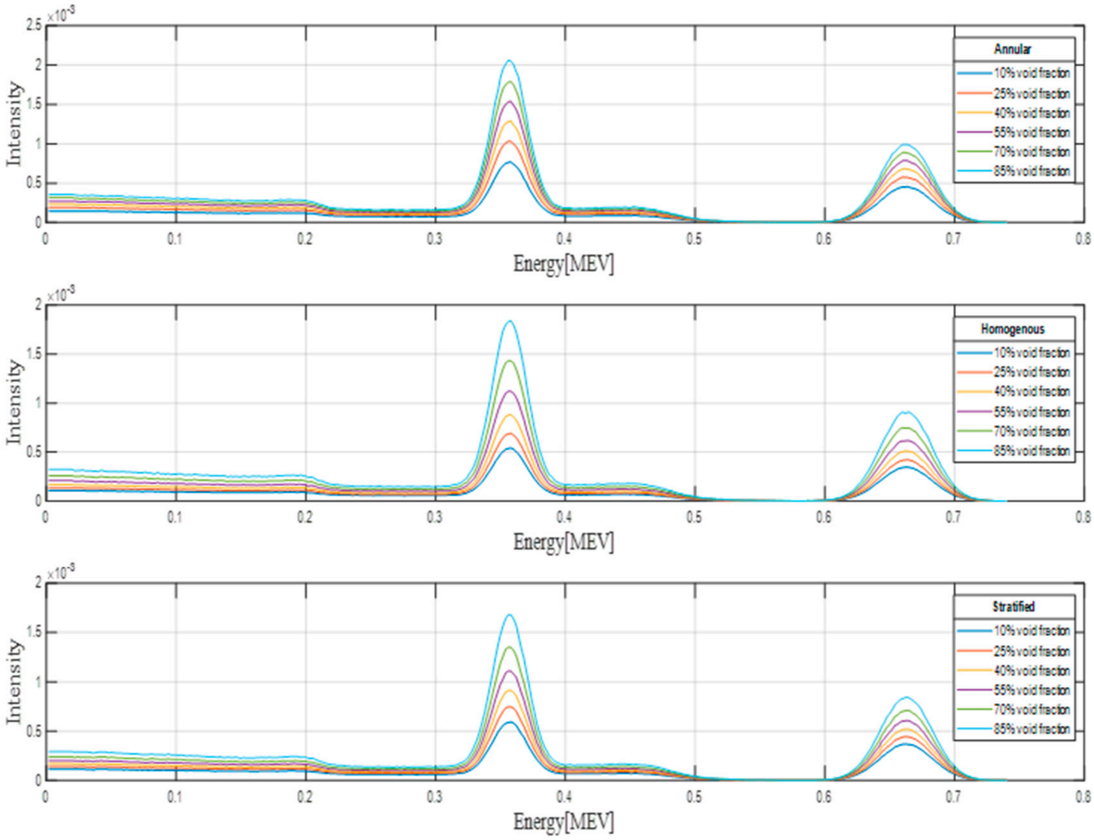

Figure 4. Recorded signal by the detector for all three simulated regimes at a 1-cm scale thickness in different void fractions.

3. Feature Extraction

Elimination of useless data, reduction of size, facilitation of the training process, and generalization of data can be considered as goals of feature extraction. Using these extracted features has a better result on the raw data than using machine learning directly, and makes the interpretation of data simpler. The schematic diagram of this procedure can be seen in Figure 5.

Figure 5. Schematic outline of the proposed feature extraction.

Data analysis may be very difficult when the amount of data is huge. Feature extraction in the domain of time, frequency, and time−frequency are among the various methods of feature extraction. Of course, these are not the only methods, and there are several methods that could be implemented to decrease the dimensionality of the data. In the present study, frequency domain feature extraction was performed, and the received signal was converted to the frequency domain using FTT (Equation (1) [19]). Then, the first to fourth dominant frequencies were extracted.

$$Y(k) = \sum_{J=1}^{n} x(J) w_n^{(y-1)(k-1)} \tag{1}$$

where $Y(k) = FFT(X)$ and $w\_n = e\hat{}((-2\pi i)/n)$ is one of n roots of unity.

As mentioned earlier, one detector was utilized in present investigation and four features were extracted from it. So, these four features were utilized to train NNs. The converted signals of all three flow regimes to the frequency domain at a 1 cm scale thickness are shown in Figure 6.

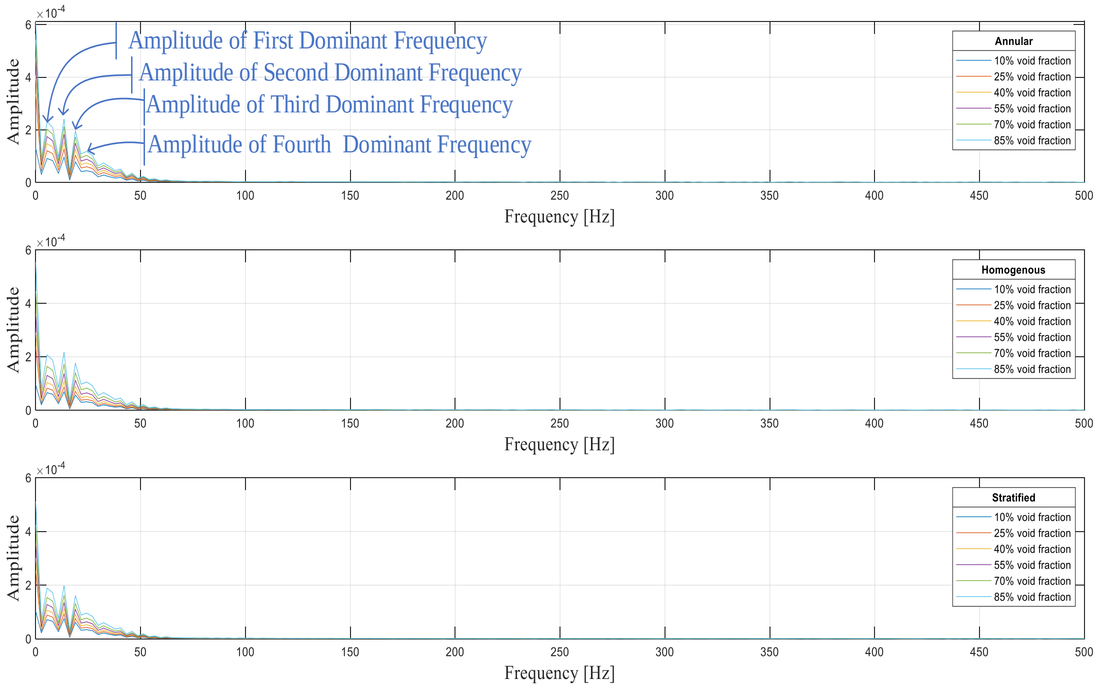

Figure 6. Converted signals into the frequency domain for a scale thickness of 1 cm.

4. RBF Neural Network

In recent years, different advanced computational approaches have been applied in various fields of study, such as fluid mechanic engineering [20–28], chemical engineering [29–33], electrical engineering [34–59], computer engineering [60–76], civil engineering [77–79], petroleum engineering [80–94], energy engineering [95–101], mathematics [102–110], medical and pharmaceutical [111–116]. It has been proved that ANN is one of the most powerful computational approaches. In addition, RBF has become one of the most widely used types of neural networks due to the various applications that have been developed for it; therefore, it is the most important competitor for multilayer perceptron. The main architecture of RBF consists of three layers. The input layer is a puller layer and with no calculation occurring in it. The second layer (hidden layer) establishes a nonlinear conformity between the input space and another space with a larger dimension. Finally, third layer generates a weighted sum along with a linear output. Such an output would be useful if RBF was used to approximate the function. An exclusive trait of RBF is processing that is done in the hidden layer. Making clusters from input space patterns is a basic idea of this process. In addition, this distance measurement is done nonlinearly, so if a pattern is located in an area adjacent to the center of a cluster, the generated value will be close to 1. The value obtained outside this area is significantly reduced. The important point is that this region is radially symmetric around the center of the cluster, so the nonlinear function becomes a known function of the radial base. The most common form of the radial base function is as follows [117]:

$$\varphi(r) = \exp\left[-\frac{r^2}{2\sigma^2}\right] \tag{2}$$

In RBF, r is the numerical value of the distance from the center of the cluster. Equation (2) shows a normal bell-shaped curve. Usually, the measured distance to the center of the cluster is the Euclidean distance. For each neuron in the hidden layer, the weights show the coordinates of the center of the cluster. Therefore, once a neuron receives an X input pattern, the distance is obtained using the following equation [55]:

$$r_j = \sqrt{\sum_{i=1}^{n} \left(x_i - w_{ij}\right)^2} \tag{3}$$

Therefore, the output of jth neuron in the hidden layer is as follows:

$$\varnothing_j = \exp\left[-\frac{\sum_{i=1}^{n} \left(x_i - w_{ij}\right)^2}{2\sigma^2}\right] \tag{4}$$

The variable σ is defined as the width or radius of the bell curve, and is sometimes necessarily determined experimentally. When the distance from the center of the normal curve reaches σ, the output decreases from 1 to 0.6.

The hidden layer includes some units which are weighted, and these weights are related to the vector that represents the center of the cluster. Weights can be obtained using traditional methods like the K-Mean or methods based on the Kohonen algorithm. In any case, the training is done non-supervised, but the number of expected clusters (k) is pre-selected, and then these algorithms obtain the best fit for these clusters. In this research, MATLAB 2018b software was used to extract the mentioned characteristics and design the RBF neural network. In MATLAB software, there are many different toolboxes for neural network training, but in designing this network, no pre-designed toolbax was used for designing the RBF network in order for more freedom of action, and all steps of neural network training were programmed. It is necessary to say that the preset function of newrb (available in the MATLAB software) was used to train the network.

Training dataset: The sample of data utilized to fit the model. The dataset that is used to train the model. The model sees and learns from this data.

Testing dataset: The sample of data utilized to provide an unbiased evaluation of a final model fit on the training dataset.

5. Results and Discussion

Two neural networks of RBF were designed in this study, with the aim of determining the type of flow patterns and estimating the gas volume percentages independent of the thickness of scale in the pipe. The structure of these networks is shown in Figure 7. The inputs of these networks were the amplitude of the first to fourth dominant frequencies of the received signal, and their outputs were the void fraction and type of flow patterns. The type of flow regimes in the classifier network were shown with numbers 1, 2, and 3. In addition, the numerical ranges for each of the regimes were defined as follows. Numbers between 0.5 and 1.5 returned to 1. Numbers between 1.5 and 2.5 indicated a homogeneous regime, and numbers in the range 2.5 to 3.5 indicated a stratified regime.

The predictor network performance for training and testing data can be seen in Figure 9. This figure displays four graphs fir the f fitting, regression, error, and error histogram. In the fitting diagram, the optimal output and the output predicted by the neural network are plotted on a diagram (obviously, the greater the compatibility of these two graphs, the higher the accuracy of the network). In the regression diagram, the network output is displayed as black circles and the desired output is displayed as a blue line. The error diagram shows the difference between the network output data and the desired data. In addition, the error histogram shows the error scatter. In addition, four error criteria, namely mean square error (MSE), RMSE, mean absolute error (MAE), and mean relative error (MRE), were calculated to calculate the error rate of this network as follows:

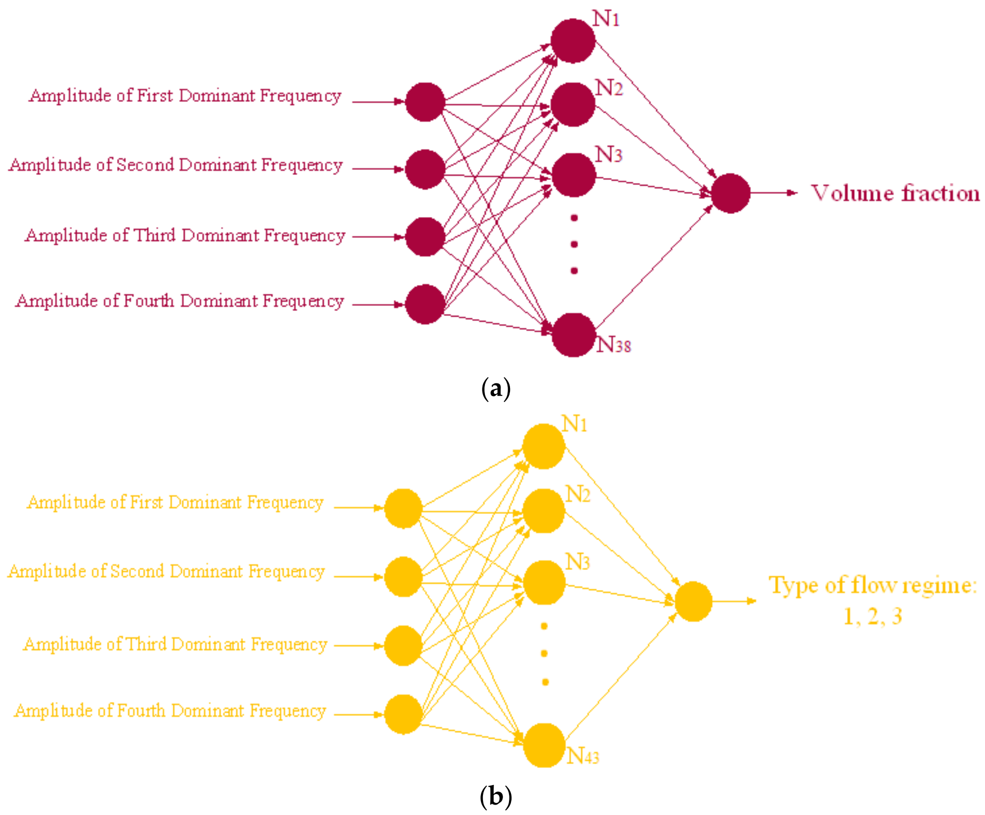

Figure 7. Implemented network structure: (**a**) predictor network and (**b**) classifier network.

A confusion matrix was implemented to represent the performance of the classifier network. This matrix can be seen for both the training and testing datasets in Figure 8, which shows 100% accuracy of the trained network.

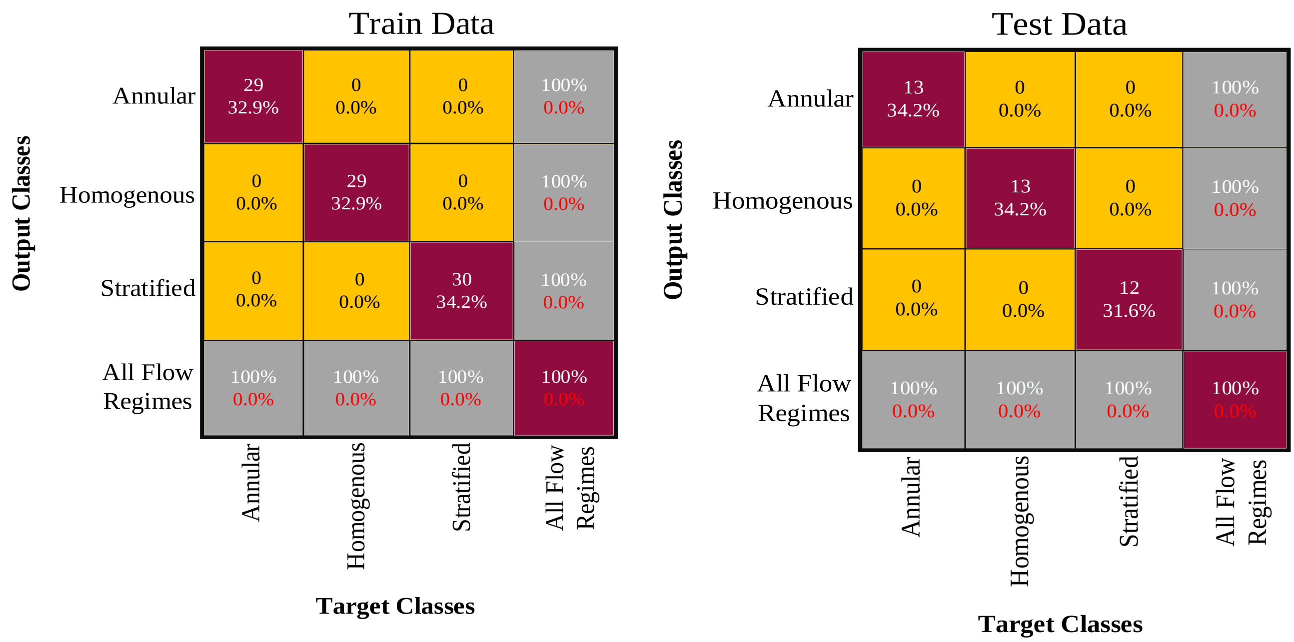

Figure 8. Performance of the classifier network.

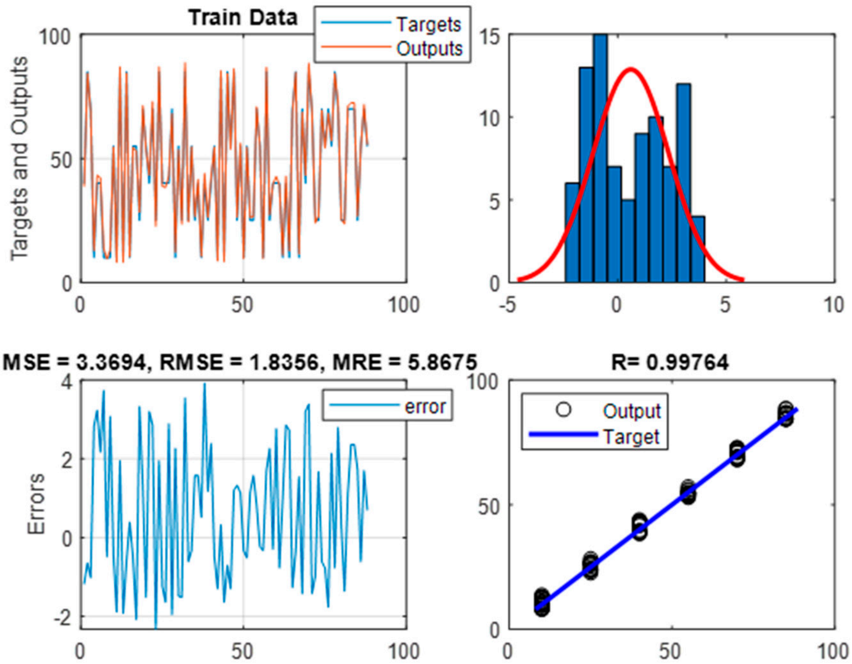

(**a**)

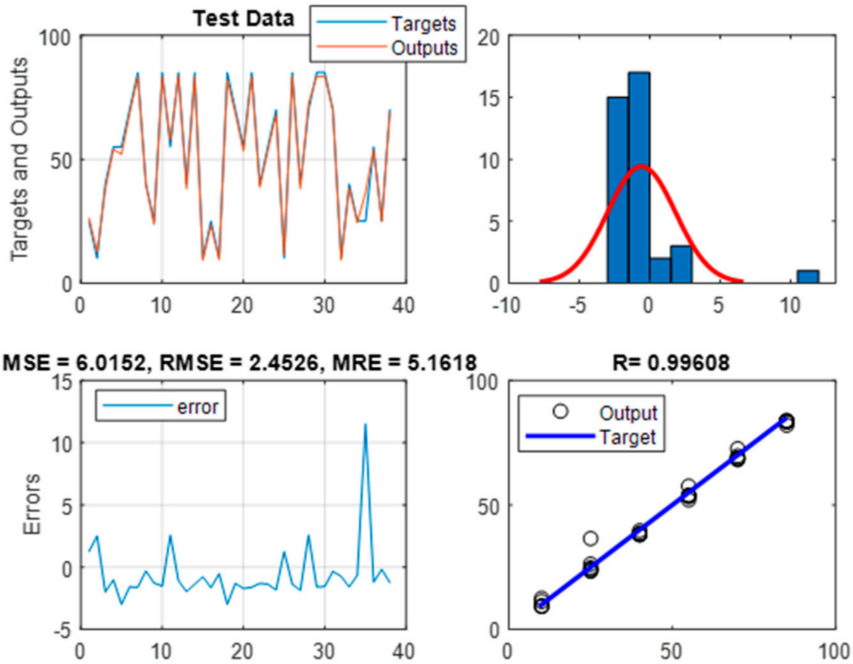

(**b**)

Figure 9. Performance of predictor network: (**a**) train and (**b**) test.

The specifications and accuracy of the trained networks can be seen in Table 1.

$$MRE\% = 100 \times \frac{1}{N}\sum_{j=1}^{N}\left|\frac{X_j(Exp) - X_j(Pred)}{X_j(Pred)}\right| \quad (5)$$

$$RMSE = \left[\frac{\sum_{j=1}^{N} \left(X_j(Exp) - X_j(Pred) \right)^2}{N} \right]^{0.5} \quad (6)$$

$$MSE = \frac{\sum_{j=1}^{N} \left(X_j(Exp) - X_j(Pred) \right)^2}{N} \quad (7)$$

$$MAE\% = \frac{1}{N} \sum_{j=1}^{N} \left| X_j(Exp) - X_j(Pred) \right| \quad (8)$$

where N is the number of data, and *X (Exp)* and *X (Pred)* stand for the experimental and predicted (ANN) values, respectively.

Table 1. Specifications of the designed networks.

	Predictor Network		**Classifier Network**	
Goal of MSE	0		0	
RBF spread	5		4	
Number of neuron in hidden layer	38		43	
CalculCalculated MSE	Train data	Test data	Train data	Test data
	3.36	6.015	0	0
Calculated RMSE	1.83	2.45	0	0
Calculated MAE	1.57	1.72	0	0
Calculated MRE%	5.86	5.16	0	0

6. Conclusions

In the present investigation, an attempt was made to present a manner for predicting the volume percentage and flow pattern in scaled oil pipelines based on a non-invasive method with a creative structure based on gamma radiation. In this regard, using the Monte Carlo code, a dual-energy source was simulated on one side of the oil transfer pipe and a detector on the other side. This process was performed to simulate different flow regimes in different volume percentages, as well as to model the thickness of the scale inside the tube. The feature extraction routine in the frequency domain, after all the simulations and data collection, was used to better decipher the collected data. The extracted features, which included the amplitude of the first to fourth dominant frequencies, were considered as neural network inputs. The prediction of volume percentage with RMSE less than 1.83 and fully classifying flow regimes were the results of the two designed neural networks. The number of detectors was decreased to one, resulting in a simplified system and reduced costs. This reduction was due to feature extraction method, which is an advantage over previous works. The results of this investigation show that the proposed process can be used in oil and petrochemical industries to measure the volume percentages and detect the fluid flow regimes.

Author Contributions: Conceptualization, E.N.; methodology, S.N. and E.E.-Z.; software, A.M.M. and J.W.G.G.; data curation, A.M.M.; writing—original draft preparation, J.W.G.G. and A.M.I.; writing—review and editing, S.M.A. and S.N.; investigation, S.M.A. and S.N.; visualization, J.W.G.G. and A.M.I.; supervision, E.N.; resource, A.S.S.; validation, A.S.S.; funding acquisition, E.E.-Z. and A.M.I. All authors have read and agreed to the published version of the manuscript.

Funding: We acknowledge support by the Open Access Publication Fund of the Thueringer Universitaets- und Landesbibliothek Jena; The Deanship of Scientific Research at King Khalid University through General Research Project under grant number (GRP-20-41 /2020); and the Deputyship for Research and Innovation of the Saudi Ministry of Education via its funding for the PSAU Advanced Computational Intelligence & Intelligent Systems Engineering (ACIISE) Research Group Project Number IF-PSAU-2021/01/18316.

Data Availability Statement: Data are contained within the article.

Conflicts of Interest: The authors declare no conflict of interest.

References

1. Abro, E.; Khoryakov, V.A.; Johansen, G.A. Determination of Void Fraction and Flow Regime Using a Neural Network Trained on Simulated Data Based on Gamma-Ray Densitometry. *Meas. Sci. Technol.* **1999**, *10*, 619–630.
2. Sattari, M.A.; Roshani, G.H.; Hanus, R. Improving the structure of two-phase flow meter using feature extraction and GMDH neural network. *Radiat. Phys. Chem.* **2020**, *171*, 108725. [CrossRef]
3. Oliveira, D.F.; Nascimento, J.R.; Marinho, C.A.; Lopes, R.T. Gamma transmission system for detection of scale in oil exploration pipelines. *Nucl. Instrum. Methods Phys. Res. Sect. A Accel. Spectrometers Detect. Assoc. Equip.* **2015**, *784*, 616–620. [CrossRef]
4. Roshani, M.; Phan, G.T.; Ali, P.J.M.; Roshani, G.H.; Hanus, R.; Duong, T.; Corniani, E.; Nazemi, E.; Kalmoun, E.M. Evaluation of flow pattern recognition and void fraction measurement in two phase flow independent of oil pipeline's scale layer thickness. *Alex. Eng. J.* **2021**, *60*, 1955–1966. [CrossRef]
5. Alamoudi, M.; Sattari, M.A.; Balubaid, M.; Eftekhari-Zadeh, E.; Nazemi, E.; Taylan, O.; Kalmoun, E.M. Application of Gamma Attenuation Technique and Artificial Intelligence to Detect Scale Thickness in Pipelines in Which Two-Phase Flows with Different Flow Regimes and Void Fractions Exist. *Symmetry* **2021**, *13*, 1198. [CrossRef]
6. Roshani, G.H.; Nazemi, E.; Feghhi, S.A.H.; Setayeshi, S. Flow regime identification and void fraction prediction in two-phase flows based on gamma ray attenuation. *Measurement* **2015**, *62*, 25–32. [CrossRef]
7. Nazemi, E.; Roshani, G.H.; Feghhi, S.A.H.; Gholipour Peyvandi, R.; Setayeshi, S. Precise Void Fraction Measurement in Two-Phase Flows Independent of the Flow Regime using gamma-ray attenuation. *Nucl. Eng. Technol.* **2016**, *48*, 64–71. [CrossRef]
8. Karami, A.; Roshani, G.H.; Salehizadeh, A.; Nazemi, E. The fuzzy logic application in volume fractions prediction of the annular three-phase flows. *J. Nondestr. Eval.* **2017**, *36*, 35. [CrossRef]
9. Roshani, M.; Sattari, M.A.; Ali, P.J.M.; Roshani, G.H.; Nazemi, B.; Corniani, E.; Nazemi, E. Application of GMDH neural network technique to improve measuring precision of a simplified photon attenuation based two-phase flowmeter. *Flow Meas. Instrum.* **2020**, *75*, 101804. [CrossRef]
10. Sætre, C.; Tjugum, S.A.; Johansen, G.A. Tomographic segmentation in multiphase flow measurement. *Radiat. Phys. Chem.* **2014**, *95*, 420–423. [CrossRef]
11. Karami, A.; Roshani, G.H.; Khazaei, A.; Nazemi, E.; Fallahi, M. Investigation of different sources in order to optimize the nuclear metering system of gas–oil–water annular flows. *Neural Comput. Appl.* **2020**, *32*, 3619–3631. [CrossRef]
12. Mosorov, V.; Zych, M.; Hanus, R.; Sankowski, D.; Saoud, A. Improvement of Flow Velocity Measurement Algorithms Based on Correlation Function and Twin Plane Electrical Capacitance Tomography. *Sensors* **2020**, *20*, 306. [CrossRef] [PubMed]
13. Salgado, C.M.; Brandão, L.E.B.; Conti, C.C.; Salgado, W.L. Density prediction for petroleum and derivatives by gamma-ray attenuation and artificial neural networks. *Appl. Radiat. Isot.* **2016**, *116*, 143–149. [CrossRef] [PubMed]
14. Roshani, M.; Sattari, M.A.; Ali, P.J.M.; Roshani, G.H.; Nazemi, B.; Corniani, E.; Phan, N.-H.; Tran, H.-N.; Nazemi, E. X-ray tube with artificial neural network model as a promising alternative for radioisotope source in radiation based two phase flowmeters. *Appl. Radiat. Isot.* **2020**, *164*, 109255. [CrossRef] [PubMed]
15. Biswal, J.; Pant, H.J.; Goswami, S.; Samantray, J.S.; Sharma, V.K.; Sarma, K.S.S. Measurement of flow rates of water in large diameter pipelines using radiotracer dilution method. *Flow Meas. Instrum.* **2018**, *59*, 194–200. [CrossRef]
16. Candeias, J.P.; De Oliveira, D.F.; Dos Anjos, M.J.; Lopes, R.T. Scale analysis using X-ray microfluorescence and computed radiography. *Radiat. Phys. Chem.* **2014**, *95*, 408–411. [CrossRef]
17. Alanazi, A.K.; Alizadeh, S.M.; Nurgalieva, K.S.; Nesic, S.; Grimaldo Guerrero, J.W.; Abo-Dief, H.M.; Eftekhari-Zadeh, E.; Nazemi, E.; Narozhnyy, I.M. Application of Neural Network and Time-Domain Feature Extraction Techniques for Determining Volumetric Percentages and the Type of Two Phase Flow Regimes Independent of Scale Layer Thickness. *Appl. Sci.* **2022**, *12*, 1336. [CrossRef]
18. Pelowitz, D.B. *MCNP-X TM User's Manual*, version 2.5.0; LA-CP-05e0369; Los Alamos National Laboratory: Los Alamos, NM, USA, 2005.
19. Nussbaumer, H.J. The Fast Fourier Transform. In *Fast Fourier Transform and Convolution Algorithms*; Springer: Berlin, Germany, 1981; pp. 80–111.
20. Roshani, G.H.; Feghhi, S.A.H.; Mahmoudi-Aznaveh, A.; Nazemi, E.; Adineh-Vand, A. Precise volume fraction prediction in oil-water-gas multiphase flows by means of gamma-ray attenuation and artificial neural networks using one detector. *Measurement* **2014**, *51*, 34–41. [CrossRef]
21. Tang, L.; Zhang, Y.; Li, C.; Zhou, Z.; Nie, X.; Chen, Y.; Cao, H.; Liu, B.; Zhang, N.; Said, Z.; et al. Biological Stability of Water-Based Cutting Fluids: Progress and Application. *Chin. J. Mech. Eng.* **2022**, *35*, 3. [CrossRef]
22. Nazemi, E.; Feghhi, S.; Roshani, G.; Setayeshi, S.A.; Peyvandi, R.G. A radiation-based hydrocarbon two-phase flow meter for estimating of phase fraction independent of liquid phase density in stratified regime. *Flow Meas. Instrum.* **2015**, *46*, 25–32. [CrossRef]
23. Saberinejad, H.; Keshavarz, A.; Payandehdoost, M.; Azmoodeh, M.R.; Batooei, A. Numerical study of heat transfer performance in a pipe partially filled with non-uniform porous media under LTNE condition. *Int. J. Numer. Methods Heat Fluid Flow* **2018**, *28*, 1845–1865. [CrossRef]
24. Roshani, G.H.; Nazemi, E.; Feghhi, S.A.H. Investigation of using 60Co source and one detector for determining the flow regime and void fraction in gas-liquid two-phase flows. *Flow Meas. Instrum.* **2016**, *50*, 73–79. [CrossRef]
25. Yang, M.; Li, C.; Luo, L.; Li, R.; Long, Y. Predictive model of convective heat transfer coefficient in bone micro-grinding using nanofluid aerosol cooling. *Int. Commun. Heat Mass Transf.* **2021**, *125*, 105317. [CrossRef]

26. Roshani, G.H.; Nazemi, E.; Roshani, M.M. Flow regime independent volume fraction estimation in three-phase flows using dual-energy broad beam technique and artificial neural network. *Neural Comput. Appl.* **2016**, *28*, 1265–1274. [CrossRef]
27. Nazemi, E.; Roshani, G.H.; Feghhi, S.A.H.; Setayeshi, S.; Eftekhari Zadeh, E.; Fatehi, A. Optimization of a method for identifying the flow regime and measuring void fraction in a broad beam gamma-ray attenuation technique. *Int. J. Hydrog. Energy* **2016**, *41*, 7438–7444. [CrossRef]
28. Roshani, G.; Nazemi, E.; Roshani, M. Usage of two transmitted detectors with optimized orientation in order to three phase flow metering. *Measurement* **2017**, *100*, 122–130. [CrossRef]
29. Khounani, Z.; Hosseinzadeh-Bandbafha, H.; Nazemi, F.; Shaeifi, M.; Karimi, K.; Tabatabaei, M.; Aghbashlo, M.; Lam, S.S. Exergy analysis of a whole-crop safflower biorefinery: A step towards reducing agricultural wastes in a sustainable manner. *J. Environ. Manag.* **2021**, *279*, 111822. [CrossRef]
30. Gao, T.; Li, C.; Yang, M.; Zhang, Y.; Jia, D.; Ding, W.; Debnath, S.; Yu, T.; Said, Z.; Wang, J. Mechanics analysis and predictive force models for the single-diamond grain grinding of carbon fiber reinforced polymers using CNT nano-lubricant. *J. Mater. Process. Technol.* **2021**, *290*, 116976. [CrossRef]
31. Zhang, Z.; Sui, M.; Li, C.; Zhou, Z.; Liu, B.; Chen, Y.; Said, Z.; Debnath, S.; Sharma, S. Residual stress of MoS2 nano-lubricant grinding cemented carbide. *Int. J. Adv. Manuf. Technol.* **2021**, 1–15. [CrossRef]
32. Gao, T.; Li, C.; Wang, Y.; Liu, X.; An, Q.; Li, H.N.; Zhang, Y.; Cao, H.; Liu, B.; Wang, D.; et al. Carbon fiber reinforced polymer in drilling: From damage mechanisms to suppression. *Compos. Struct.* **2022**, *286*, 115232. [CrossRef]
33. Nazemi, F.; Karimi, K.; Denayer, J.F.; Shafiei, M. Techno-economic aspects of different process approaches based on brown macroalgae feedstock: A step toward commercialization of seaweed-based biorefineries. *Algal Res.* **2021**, *58*, 102366. [CrossRef]
34. Roshani, S.; Roshani, S. Two-Section Impedance Transformer Design and Modeling for Power Amplifier Applications. *Appl. Comput. Electromagn. Soc. J.* **2017**, *32*, 1042–1047.
35. Lalbakhsh, A.; Lotfi Neyestanak, A.A.; Naser-Moghaddasi, M. Microstrip hairpin bandpass filter using modified Minkowski fractal-shape for suppression of second harmonic. *IEICE Trans. Electron.* **2012**, *E95-C*, 378–381. [CrossRef]
36. Hayerikhiyavi, M.; Dimitrovski, A. A Practical Assessment of the Power Grid Inertia Constant Using PMUs. In Proceedings of the 2020 52nd North American Power Symposium (NAPS), virtual, 11–14 April 2021; pp. 1–5.
37. Pirasteh, A.; Roshani, S.; Roshani, S. Compact microstrip lowpass filter with ultrasharp response using a square-loaded mod-ified T-shaped resonator. *Turk. J. Electr. Eng. Comput. Sci.* **2018**, *26*, 1736–1746. [CrossRef]
38. Lalbakhsh, A.; Afzal, M.U.; Esselle, K.P.; Smith, S.L. Low-cost nonuniform metallic lattice for rectifying aperture near-field of electromagnetic bandgap resonator antennas. *IEEE Trans. Antennas Propag.* **2020**, *68*, 3328–3335. [CrossRef]
39. Roshani, S.; Roshani, S. A compact coupler design using meandered line compact microstrip resonant cell (MLCMRC) and bended lines. *Wirel. Netw.* **2021**, *27*, 677–684. [CrossRef]
40. Lalbakhsh, A.; Ghaderi, A.; Mohyuddin, W.; Simorangkir, R.B.V.B.; Bayat-Makou, N.; Ahmad, M.S.; Lee, G.H.; Kim, K.W. A Compact C-Band Bandpass Filter with an Adjustable Dual-Band Suitable for Satellite Communication Systems. *Electronics* **2020**, *9*, 1088. [CrossRef]
41. Roshani, S.; Roshani, S. Design of a very compact and sharp bandpass diplexer with bended lines for GSM and LTE applica-tions. *AEU Int. J. Electron. Commun.* **2019**, *99*, 354–360. [CrossRef]
42. Lalbakhsh, A.; Alizadeh, S.M.; Ghaderi, A.; Golestanifar, A.; Mohamadzade, B.; Jamshidi, M.B.; Mandal, K.; Mohyuddin, W. A design of a dual-band bandpass filter based on modal analysis for modern communication systems. *Electronics* **2020**, *9*, 1770. [CrossRef]
43. Roshani, S.; Roshani, S.; Zarinitabar, A. A modified Wilkinson power divider with ultra harmonic suppression using open stubs and lowpass filters. *Analog. Integr. Circuits Signal Process.* **2019**, *98*, 395–399. [CrossRef]
44. Lalbakhsh, A.; Afzal, M.U.; Hayat, T.; Esselle, K.P.; Manda, K. All-metal wideband metasurface for near-field transformation of medium-to-high gain electromagnetic sources. *Sci. Rep.* **2021**, *11*, 9421. [CrossRef]
45. Jamshidi, M.B.; Siahkamari, H.; Roshani, S.; Roshani, S. A compact Gysel power divider design using U-shaped and T-shaped reso-nators with harmonics suppression. *Electromagnetics* **2019**, *39*, 491–504. [CrossRef]
46. Lalbakhsh, A.; Jamshidi, M.B.; Siahkamari, H.; Ghaderi, A.; Golestanifar, A.; Linhart, R.; Talla, J.; Simorangkir, R.B.; Mandal, K. A compact lowpass filter for satellite communication systems based on transfer function analysis. *AEU Int. J. Electron. Commun.* **2020**, *124*, 153318. [CrossRef]
47. Jamshidi, M.B.; Roshani, S.; Talla, J.; Roshani, S.; Peroutka, Z. Size reduction and performance improvement of a microstrip Wilkinson power divider using a hybrid design technique. *Sci. Rep.* **2021**, *11*, 7773. [CrossRef]
48. Pirasteh, A.; Roshani, S.; Roshani, S. A modified class-F power amplifier with miniaturized harmonic control circuit. *AEU Int. J. Electron. Commun.* **2018**, *97*, 202–209. [CrossRef]
49. Roshani, S.; Roshani, S. Design of a high efficiency class-F power amplifier with large signal and small signal measurements. *Measurement* **2020**, *149*, 106991. [CrossRef]
50. Lalbakhsh, A.; Mohamadpour, G.; Roshani, S.; Ami, M.; Roshani, S.; Sayem, A.S.M.; Alibakhshikenari, M.; Koziel, S. Design of a compact planar transmission line for miniaturized rat-race coupler with harmonics suppression. *IEEE Access* **2021**, *9*, 129207–129217. [CrossRef]
51. Roshani, S.; Roshani, S. Design of a compact LPF and a miniaturized Wilkinson power divider using aperiodic stubs with harmonic suppression for wireless applications. *Wirel. Netw.* **2019**, *26*, 1493–1501. [CrossRef]

52. Pirasteh, A.; Roshani, S.; Roshani, S. Design of a miniaturized class F power amplifier using capacitor loaded transmission lines. *Frequenz* **2020**, *74*, 145–152. [CrossRef]
53. Lotfi, S.; Roshani, S.; Roshani, S.; Gilan, M.S. Wilkinson power divider with band-pass filtering response and harmonics suppression using open and short stubs. *Frequenz* **2020**, *74*, 169–176. [CrossRef]
54. Hookari, M.; Roshani, S.; Roshani, S. Design of a low pass filter using rhombus-shaped resonators with an analyticallc equivalent circuit. *Turk. J. Electr. Eng. Comput. Sci.* **2020**, *28*, 865–874. [CrossRef]
55. Roshani, S.; Koziel, S.; Roshani, S.; Jamshidi, M.B.; Parandin, F.; Szczepanski, S. Design of a Patch Power Divider with Simple Structure and Ultra-Broadband Harmonics Suppression. *IEEE Access* **2021**, *9*, 165734–165744. [CrossRef]
56. Pourbemany, J.; Mirjalily, G.; Abouei, J.; Raouf, A.H.F. Load Balanced Ad-Hoc On-Demand Routing Basedon Weighted Mean Queue Length Metric. In Proceedings of the Iranian Conference on Electrical Engineering (ICEE), Mashhad, Iran, 8–10 May 2018; pp. 470–475.
57. Lotfi, S.; Roshani, S.; Roshani, S. Design of a miniaturized planar microstrip Wilkinson power divider with harmonic cancellation. *Turk. J. Electr. Eng. Comput. Sci.* **2020**, *28*, 3126–3136. [CrossRef]
58. Bavandpour, S.K.; Roshani, S.; Pirasteh, A.; Roshani, S.; Seyedi, H. A compact lowpass-dual bandpass diplexer with high output ports isolation. *AEU-Int. J. Electron. Commun.* **2021**, *135*, 153748. [CrossRef]
59. Roshani, S.; Dehghani, K.; Roshani, S. A Lowpass Filter Design Using Curved and Fountain Shaped Resonators. *Frequenz* **2019**, *73*, 267–272. [CrossRef]
60. Dudek, G. Short-Term Load Forecasting Using Neural Networks with Pattern Similarity-Based Error Weights. *Energies* **2021**, *14*, 3224. [CrossRef]
61. Mahum, R.; Rehman, S.U.; Okon, O.D.; Alabrah, A.; Meraj, T.; Rauf, H.T. A Novel Hybrid Approach Based on Deep CNN to Detect Glaucoma Using Fundus Imaging. *Electronics* **2022**, *11*, 26. [CrossRef]
62. Lalbakhsh, A.; Afzal, M.U.; Esselle, K. Simulation-driven particle swarm optimization of spatial phase shifters. In Proceedings of the 2016 International Conference on Electromagnetics in Advanced Applications (ICEAA), Cairns, Australia, 19–23 September 2016.
63. Yan, A.; Fan, Z.; Ding, L.; Cui, J.; Huang, Z.; Wang, Q.; Zheng, H.; Girard, P.; Wen, X. Cost-Effective and Highly Reliable Circuit Components Design for Safety-Critical Applications. *IEEE Trans. Aerosp. Electron. Syst.* **2021**, 1. [CrossRef]
64. Sadeqi, S.; Xiros, N.; Rouhi, S.; Ioup, J.; VanZwieten, J.; Sultan, C. WAVELET TRANSFORMATION ANALYSIS APPLIED TO INCOMPRESSIBLE FLOW FIELD ABOUT A SOLID CYLINDER. In Proceedings of the ASTFE 5–6th Thermal and Fluids Engineering Conference (TFEC), virtual, 26–28 May 2021.
65. Yan, A.; Xu, Z.; Feng, X.; Cui, J.; Chen, Z.; Ni, T.; Huang, Z.; Girard, P.; Wen, X. Novel Quadruple-Node-Upset-Tolerant Latch Designs with Optimized Overhead for Reliable Computing in Harsh Radiation Environments. *IEEE Trans. Emerg. Top. Comput.* **2020**, 1. [CrossRef]
66. Kim, S.; Akpudo, U.E.; Hur, J.-W. A Cost-Aware DNN-Based FDI Technology for Solenoid Pumps. *Electronics* **2021**, *10*, 2323. [CrossRef]
67. Jamshidi, M.; Lalbakhsh, A.; Talla, J.; Peroutka, Z.; Hadjilooei, F.; Lalbakhsh, P.; Jamshidi, M.; La Spada, L.; Mirmozafari, M.; Dehghani, M.; et al. Artificial intelligence and COVID-19: Deep learning approaches for diagnosis and treatment. *IEEE Access* **2020**, *8*, 109581–109595. [CrossRef]
68. Chapnevis, A.; Sadeghiyan, B. A Secure Two-Party Computation Protocol for Intersection Detection between Two Convex Hulls. *arXiv* **2020**, arXiv:2011.00319.
69. Walid, W.; Awais, M.; Ahmed, A.; Masera, G.; Martina, M. Real-time implementation of fast discriminative scale space tracking algorithm. *J. Real-Time Image Process.* **2021**, *18*, 2347–2360. [CrossRef]
70. Vesel, C.; Rashidisabet, H.; Zulueta, J.; Stange, J.P.; Duffecy, J.; Hussain, F.; Piscitello, A.; Bark, J.; A Langenecker, S.; Young, S.; et al. Effects of mood and aging on keystroke dynamics metadata and their diurnal patterns in a large open-science sample: A BiAffect iOS study. *J. Am. Med. Inform. Assoc.* **2020**, *27*, 1007–1018. [CrossRef] [PubMed]
71. Ramtin, A.R.; Nain, P.; Towsley, D.; e Silva, E.D.S.; Menasche, D.S. Are covert ddos attacks facing multi-featuredetectors feasible. *ACM SIGMETRICS Perform. Eval. Rev.* **2021**, *49*, 33–35. [CrossRef]
72. Shiri, A. A Novel Implementation of CORDIC Algorithm Based on Dynamic Microrotation Generation. *Mapta J. Electr. Comput. Eng. MJECE* **2021**, *3*, 17–27.
73. Liu, L.; Xiang, H.; Li, X. A novel perturbation method to reduce the dynamical degradation of digital chaotic maps. *Nonlinear Dyn.* **2021**, *103*, 1099–1115. [CrossRef]
74. Pourjabar, S.; Choi, G.S. A High-Throughput Multi-Mode LDPC Decoder for 5G NR. *arXiv* **2021**, arXiv:2102.13228.
75. Luo, G.; Yuan, Q.; Zhou, H.; Cheng, N.; Liu, Z.; Yang, F.; Shen, X.S. Cooperative vehicular content distribution in edge computing assisted 5G-VANET. *China Commun.* **2018**, *15*, 1–17. [CrossRef]
76. Hookari, M.; Roshani, S.; Roshani, S. High-efficiency balanced power amplifier using miniaturized harmonics suppressed coupler. *Int. J. RF Microw. Comput.-Aided Eng.* **2020**, *30*, e22252. [CrossRef]
77. Nazemi, B.; Rafiean, M. Forecasting house prices in Iran using GMDH. *Int. J. Hous. Mark. Anal.* **2021**, *14*, 555–568. [CrossRef]
78. Moradi, M.J.; Hariri-Ardebili, M.A. Developing a Library of Shear Walls Database and the Neural Network Based Predictive Meta-Model. *Appl. Sci.* **2019**, *9*, 2562. [CrossRef]

79. Nazemi, B.; Rafiean, M. Modelling the affecting factors of housing price using GMDH-type artificial neural networks in Isfa-han city of Iran. *Int. J. Hous. Mark. Anal.* **2021**, *15*, 4–18. [CrossRef]
80. Roshani, G.; Nazemi, E. Intelligent densitometry of petroleum products in stratified regime of two phase flows using gamma ray and neural network. *Flow Meas. Instrum.* **2017**, *58*, 6–11. [CrossRef]
81. Khaibullina, K. Technology to Remove Asphaltene, Resin and Paraffin Deposits in Wells Using Organic Solvents. In Proceedings of the SPE Annual Technical Conference and Exhibition, Dubai, United Arab Emirates, 26–28 September 2016. [CrossRef]
82. Roshani, G.; Nazemi, E.; Roshani, M. Intelligent recognition of gas-oil-water three-phase flow regime and determination of volume fraction using radial basis function. *Flow Meas. Instrum.* **2017**, *54*, 39–45. [CrossRef]
83. Nurgalieva, K.S.; Saychenko, L.A.; Riazi, M. Improving the efficiency of oil and gas wells complicated by the formation of asphalt-resin-paraffin deposits. *Energies* **2021**, *14*, 6673. [CrossRef]
84. Roshani, G.; Nazemi, E.; Roshani, M. Identification of flow regime and estimation of volume fraction independent of liquid phase density in gas-liquid two-phase flow. *Prog. Nucl. Energy* **2017**, *98*, 29–37. [CrossRef]
85. Syah, R.; Alizadeh, S.M.; Nurgalieva, K.S.; Guerrero, J.W.G.; Nasution, M.K.M.; Davarpanah, A.; Ramdan, D.; Metwally, A.S.M. A laboratory approach to measure enhanced gas recovery from a tight gas reservoir during supercritical carbon dioxide injection. *Sustainability* **2021**, *13*, 11606. [CrossRef]
86. Karami, A.; Roshani, G.H.; Nazemi, E.; Roshani, S. Enhancing the performance of a dual-energy gamma ray based three-phase flow meter with the help of grey wolf optimization algorithm. *Flow Meas. Instrum.* **2018**, *64*, 164–172. [CrossRef]
87. Khaibullina, K.S.; Sagirova, L.R.; Sandyga, M.S. Substantiation and selection of an inhibitor for preventing the formation of asphalt-resin-paraffin deposits. *Period. Tche Quim.* **2020**, *17*, 541–551. (In Portuguese) [CrossRef]
88. Roshani, G.H.; Roshani, S.; Nazemi, E.; Roshani, S. Online measuring density of oil products in annular regime of gas-liquid two phase flows. *Measurement* **2018**, *129*, 296–301. [CrossRef]
89. Roshani, G.; Hanus, R.; Khazaei, A.; Zych, M.; Nazemi, E.; Mosorov, V. Density and velocity determination for single-phase flow based on radiotracer technique and neural networks. *Flow Meas. Instrum.* **2018**, *61*, 9–14. [CrossRef]
90. Roshani, M.; Phan, G.; Faraj, R.H.; Phan, N.H.; Roshani, G.H.; Nazemi, B.; Corniani, E.; Nazemi, E. Proposing a gamma radiation based intelligent system for simultaneous analyzing and detecting type and amount of petroleum by-products. *Neural Eng. Technol.* **2021**, *53*, 1277–1283. [CrossRef]
91. Khaibullina, K.S.; Korobov, G.Y.; Lekomtsev, A.V. Development of an asphalt-resin-paraffin deposits inhibitor and substantiation of the technological parameters of its injection into the bottom-hole formation zone. *Period. Tche Quim.* **2020**, *17*, 769–781. (In Portuguese) [CrossRef]
92. Roshani, M.; Phan, G.; Roshani, G.H.; Hanus, R.; Nazemi, B.; Corniani, E.; Nazemi, E. Combination of X-ray tube and GMDH neural network as a nondestructive and potential technique for measuring characteristics of gas-oil-water three phase flows. *Measurement* **2021**, *168*, 108427. [CrossRef]
93. Tikhomirova, E.A.; Sagirova, L.R.; Khaibullina, K.S. A Review on Methods of Oil Saturation Modelling using IRAP RMS. In Proceedings of the International Conference on Innovations and Prospects of Development of Mining Machinery and Electrical Engineering 2019, Saint-Petersburg, Russia, 24–27 April 2019; Volume 378. [CrossRef]
94. Sattari, M.A.; Roshani, G.H.; Hanus, R.; Nazemi, E. Applicability of time-domain feature extraction methods and artificial intelligence in two-phase flow meters based on gamma-ray absorption technique. *Measurement* **2021**, *168*, 108474. [CrossRef]
95. Mou, J.; Duan, P.; Gao, L.; Liu, X.; Li, J. An effective hybrid collaborative algorithm for energy-efficient distributed permutation flow-shop inverse scheduling. *Future Gener. Comput. Syst.* **2022**, *128*, 521–537. [CrossRef]
96. Wang, Y.; Zou, R.; Liu, F.; Zhang, L.; Liu, Q. A review of wind speed and wind power forecasting with deep neural networks. *Appl. Energy* **2021**, *304*, 117766. [CrossRef]
97. Hosseinzadeh-Bandbafha, H.; Nazemi, F.; Khounani, Z.; Ghanavati, H.; Shafiei, M.; Karimi, K.; Lam, S.S.; Aghbashlo, M.; Tabatabaei, M. Safflower-based biorefinery producing a broad spectrum of biofuels and biochemicals: A life cycle assessment perspective. *Sci. Total Environ.* **2021**, *802*, 149842. [CrossRef]
98. Kang, Y.; Wu, Q. Pressure Calculation of Gas Hydrate in the Coastal Area of the Coastal Area Based on the Set Pair Analysis. *J. Coast. Res.* **2020**, *103* (Suppl. 1), 1018–1021. [CrossRef]
99. Nouriani, A.; Moradi, H. Smooth switching in power control of wind turbines using a combination strategy of hysteresis and modified middle regions. *Sustain. Energy Technol. Assess.* **2020**, *37*, 100585. [CrossRef]
100. Yin, Q.; Li, C.; Dong, L.; Bai, X.; Zhang, Y.; Yang, M.; Jia, D.; Li, R.; Liu, Z. Effects of Physicochemical Properties of Different Base Oils on Friction Coefficient and Surface Roughness in MQL Milling AISI 1045. *Int. J. Precis. Eng. Manuf.-Green Technol.* **2021**, *8*, 1629–1647. [CrossRef]
101. Nouriani, A.; Moradi, H. Variable speed wind turbine power control: A comparison between multiple MPPT based methods. *Int. J. Dyn. Control.* **2021**, 1–14. [CrossRef]
102. Ghanbari, B. Abundant exact solutions to a generalized nonlinear Schrödinger equation with local fractional derivative. *Math. Methods Appl. Sci.* **2021**, *44*, 8759–8774. [CrossRef]
103. Kharazmi, O.; Jahangard, S. A new family of lifetime distributions in terms of cumulative hazard rate function. *Commun. Fac. Sci. Univ. Ank. Ser. A1 Math. Stat.* **2020**, *69*, 1–22. [CrossRef]
104. Ghanbari, B. Chaotic behaviors of the prevalence of an infectious disease in a prey and predator system using fractional derivatives. *Math. Methods Appl. Sci.* **2021**, *44*, 9998–10013. [CrossRef]

105. Kharazmi, O.; Saadatinik, A.; Jahangard, S. Odd hyperbolic cosine exponential-exponential (OHC-EE) distribution. *Ann. Data Sci.* **2019**, *6*, 765–785. [CrossRef]
106. Ghanbari, B. On novel nondifferentiable exact solutions to local fractional Gardner's equation using an effective technique. *Math. Methods Appl. Sci.* **2021**, *44*, 4673–4685. [CrossRef]
107. Nabti, A.; Ghanbari, B. Global stability analysis of a fractional SVEIR epidemic model. *Math. Methods Appl. Sci.* **2021**, *44*, 8577–8597. [CrossRef]
108. Ghanbari, B. A fractional system of delay differential equation with nonsingular kernels in modeling hand-foot-mouth disease. *Adv. Differ. Equ.* **2020**, *2020*, 536. [CrossRef]
109. Nouriani, A.; McGovern, R.A.; Rajamani, R. Step Length Estimation Using Inertial Measurements Units. In Proceedings of the 2021 American Control Conference (ACC), virtual, 25–28 May 2021; pp. 666–671.
110. Ghanbari, B. On approximate solutions for a fractional prey-predator model involving the Atangana-Baleanu derivative. *Adv. Differ. Equ.* **2020**, *2020*, 679. [CrossRef]
111. Rashidisabet, H.; Thomas, P.J.; Ajilore, O.; Zulueta, J.; Moore, R.C.; Leow, A. A systems biology approach to the digital behaviorome. *Curr. Opin. Syst. Biol.* **2020**, *20*, 8–16. [CrossRef]
112. Sanaat, A.; Zafarghandi, M.S.; Ay, M.R. Design and performance evaluation of high resolution small animal PET scanner based on Monolithic Crystal: A Simulation Study. *J. Instrum.* **2019**, *14*, P01005. [CrossRef]
113. Azmoodeh, M.R.; Keshavarz, A.; Batooei, A.; Saberinejad, H.; Payandeh Doost, M.; Keshtkar, H. Experimental study and thermal analysis of a Gamma type Stirling engine for multi-objective optimization. *Automot. Sci. Eng.* **2020**, *10*, 3281–3294.
114. Sarhadi, M.; Aryan, L.; Zarei, M. The Estrogen Receptor and Breast Cancer: A Complete Review. *CRPASE Trans. Appl. Sci.* **2020**, *6*, 309–314.
115. Mostoufi, A.; Chamkouri, N.; Kordrostami, S.; Alghasibabaahmadi, E.; Mojaddami, A. 3-Hydroxypyrimidine-2, 4-dione derivatives as HIV Reverse Transcriptase-Associated RNase H Inhibitors: QSAR analysis and molecular dockingstudies. *Iran. J. Pharm. Res. IJPR* **2020**, *19*, 84.
116. Pourbemany, J.; Essa, A.; Zhu, Y. Real Time Video based Heart and Respiration Rate Monitoring. *arXiv* **2021**, arXiv:2106.02669.
117. Hartman, E.J.; Keeler, J.D.; Kowalski, J.M. Layered neural networks with Gaussian hidden units as universal approxima-tors. *Neural Comput.* **1990**, *2*, 210–215. [CrossRef]